Biophysical Journal, Volume 96

Supporting Material

Fluid Shear Induces Conformation Change in Human Blood Protein Von Willebrand Factor in Solution

Indrajeet Singh, Efrosyni Themistou, Lionel Porcar and Sriram Neelamegham

SUPPLEMENTAL MATERIAL

Table of Content

Supplemental Methods
I. Small Angle Neutron Scattering(SANS) Instrumentation
II. SANS Data Reduction
III. Molecular model of VWF response to fluid shear

Supplemental References

Supplemental Figures

SUPPLEMENTAL METHODS

I. Small Angle Neutron Scattering (SANS) instrumentation

Small angle neutron scattering experiments were performed using the 30 meter NG-3 SANS spectrometer at the NIST Center for Neutron Research (Gaithersburg, MD) ((1, 2), www.ncnr.nist.gov/instruments/ng3sans). This is an advanced small angle scattering spectroscopy instrument. Neutrons with wavelength (λ) of 6Å and spread ($\Delta\lambda/\lambda$) of 0.264 FWHM (Full Width at Half-Maximum) were used. Source distance was controlled by using 8 and 3 guides corresponding to the area detector being placed at distances of 1.95m and 10.05m respectively from the sample. Scatter intensity ($I(q)$) data were thus collected in the q-range (scattering vector range) from 0.045/nm to 3.169/nm; where q is defined as $4\pi/\lambda \mathrm{Sin}(\theta/2)$ with θ representing the scattering angle. In general, q is a measure of instrument magnification, and it is related to the length scale being studied according to length scale $\sim 2\pi/q$. In the case of our experiments, the protein size range studied varies from ~2 nm at high-q ($2\pi/q_{max}$) to ~139.6 nm at low-q ($2\pi/q_{min}$).

The ORNL (Oak Ridge National Laboratory) Couette shear cell (3) was aligned in the neutron beam path of the SANS instrument, such that the neutron beam passed through its center. This shear cell was chosen since it affords a large gap distance even for relatively small sample size, and since it is designed for long term, high shear experiments with sample evaporation losses being minimized by an "active barrier" design. The configuration we used consists of a rotating outer cylinder (the rotor) with an inner radius of 25.00mm and an inner stationary cylinder (stator) with an outer radius of 24.50mm. The neutron path in the Couette cell is made of quartz (Suprasil), which is highly transparent to cold neutrons. The sample gap (g) is 0.5mm and the sample volume required for each run is ~7 mL. In this design, the average shear rate G varies as $2\pi Rf/g$; where R is the radius of the fluid annulus (=24.75mm) and f is the cylinder's rotation frequency (rpm or rps). There is only a small ~4% variation in shear rate across the sample since the shear rate in the Couette cell varies across the gap in proportion to r^{-2}, where r is the distance of any point in the shear cell with respect to the axis of rotation. Taylor vortices do not occur in this instrument since the outer cylinder is rotated and secondary flow features are minimal (3). The operating limit for this device is the critical Reynolds number (Re_{CR}~1500) where the onset of turbulence is expected. For the case of the aqueous buffers used in our studies, shear rate is expected to be laminar up to 6000/s. To ensure that stable, linear shear in applied, a shear rate of 3000/s was not exceeded in the current study.

II. SANS Data Reduction

Raw data collected from SANS experiments were subjected to standard data reduction protocols to obtain 1-dimensional $I(q)$ versus q data. This processing of raw scattering data files was performed using the data reduction program (4) provided by the NIST Center for Neutron Research. Briefly, data reduction first involved correction of the raw data for background, detector sensitivity and scattering from the empty cell (2). Data were also placed on an absolute scale by measuring the incident beam flux. Since our protein is randomly oriented in solution and since there is no anisotropy in the scattering signal, data were radially averaged to obtain the 1-dimensional scattering intensity ($I(q)$) versus scattering vector (q) plot. Incoherent scattering due to residual hydrogen was then deleted from these data by estimating the flat baseline intensity seen at the high-q range for protein sample prior to shear, and subtracted this from the raw $I(q)$ vs. q data. The resulting corrected $I(q)$ vs. q data are presented in most cases in the main manuscript (Fig. 2, 3) and Supplemental Fig. S1.

Using the protein measurements as described in Methods, in some instances, the scattering data were normalized with respect to the solution concentration of VWF in the Couette

cell to obtain the *I*/*c* plot (Fig. 2C). Such analysis accounts for possible alterations in neutron scattering due to the loss/adhesion of VWF to the Couette cell wall.

III. Molecular model of VWF response to fluid shear

A computer model was written in order to relate experimentally observed changes in scattering patterns with potential changes in protein structure. This program was based on the Monte Carlo distance distribution chord sampling method described elsewhere (5). The computer program for this model was written in Visual Fortran (Intel) with numerical libraries from IMSL (Visual Numerics, Houston, TX).

In this model, the structure of the VWF protomer was simulated based on published experimental data. In this context, electron microscopy studies suggest that the VWF protomer has 2-fold symmetry, with each half consisting of a long flexible 34x2nm rod linked to a 35x6.5nm size large globular domain at one end, and to a second rod at the other end (6, 7) (Figure 1). The angle between the rods varies from 20-180º with an average angle of 77º. The globular domain contains the D'D3-A1-A2-A3 region while the rod region contains the B1-B2-B3-C1-C2 domains. The D4 domain lies at the junction of the rod and globular region. The CK domain forms the link between two VWF monomers at the C-terminus. Further, X-ray crystallography studies show that individual VWF A-domains have dimensions of ~4x3x4nm (8, 9). Although D-domain structures are yet unpublished, based on molecular weight it is expected that they will also be ~5nm in size. Further using sequence information, it is inferred that there are 685 amino acids in the rod section and 1365 amino acids in the globular section, including the D4 domain.

Based on the above, the VWF protomer in our computational model is assumed to consist of a pair of 34x2-nm rods linked to spherical domains at the ends. To create the rod *in silico*, a parallelopiped of dimensions 34x2x2nm was first created and divided by narrow grids spaced 0.1nm apart. Among all the grid nodes, the subset of points located within a hypothetical rod of length 34nm and diameter 2nm was selected and stored. A fixed sphere of diameter 5nm was placed at one end of the rod, and this was discretized with grids 0.1nm apart. This sphere represents the D4 domain of VWF. Next, two additional 4nm and two 5nm diameter spheres were placed at different distances from the fixed sphere. These additional spheres represent the A and D'D3 domains. One of two strategies were applied to determine the positions of the two 4nm and two 5nm spheres: i) In some cases, we randomly define 20 possible coordinates for the individual domains and then select four of these at random positions to place the A1, A2, A3 and D'D3 domains. ii) In other cases, we define specific locations for these four domains with the choice of domain coordinates being guided by the experimental data that we wish to fit. While both strategies were used during the course of this project, the later strategy was applied to obtain results in Fig. 4. Once the position for these four spheres was defined, each of these spheres was also discretized with 0.1nm grids. The co-ordinates of points within all spheres were stored. Following this selection, the dimer/protomer was constructed by duplicating the rod-sphere section just described and rotating it about the C-terminal end by an angle of 2φ. It is noted based on the above description that the density of points within the rod and sphere are identical, i.e. the grids are spaced 0.1nm apart in both sections. Computer modeling with the above structure were performed in three different contexts:

Case A: In the first case, the effect of changing the angle (2φ) between the monomer units/rods was studied. This effectively simulates the effects of VWF elongation in the absence of changes in the arrangement of domains within the globular section. For these computer modeling, the five spheres in the globular domain were fixed at predetermined points, and the angle between the rods was incrementally varied from φ= 12º to 84º in steps of 12º. Here, while 12º represents a

compact dimer, an extended dimer occurs at φ =84º. Some results from this first class of computer modeling are described in Fig. 4A-4C.

Case B: In the second case, the effect of domain rearrangement within the globular section was examined. Here, the distance of the two 5nm spheres in the globular section and the fixed D4 domain was increased from 3.5 and 10nm ('prior to shear'), to 5.5nm and 13.5nm respectively ('after shear'). In addition a small 1nm sphere was introduced in order to represent scattering due to inter-domain regions that may be separated from the fixed spheres as a result of domain rearrangement. Details on these changes along with accompanying schematics are provided in legends to Fig 4 (main manuscript). For each of these configurations, VWF with seven different φ values ranging from φ =12º to 84º in steps of 12º were constructed. Weighted average $I(q)$ data for these configurations was calculated, as described below, for each of the inter-domain configurations. These simulation results are presented in Fig. 4D-4F.

Case C: In the third case, the effect of VWF multimerization was simulated. As shown in Fig. 4G-I such multimers were generated by the attachment of protomer/dimeric VWF at the N-terminus at various angles. In these tetrameric molecules, both the dimeric units are identical to each other. The placement of spheres in the globular sections of the VWF monomers is identical. Thus, while small length scale features are not different in the various configurations generated, larger length scale dimensions are altered as a result of N-terminal multimerization.

For each of the above VWF configurations, 200,000 random nodes are selected in the protomer, in proportion to the number of amino acids in these individual sections. Thus, there were 66,829 points in the rod and 133,170 in the globular section. These points were selected using a random number generation algorithm. Using the same random number generator and the candidate nodes identified above, 200,000 node-pairs were selected within the dimeric protein. The distance between these selected pairs of nodes was measured in terms of the chord length. The length of each chord was calculated and among these the chord of maximum length (r_{max}) was identified. Next, 1000 equal-sized bins each with a length of r_{max}/1000 were created, and each of the 200,000 chords above was placed in one of these bins. The distribution function that resulted from such analysis is termed the distance distribution function, *P(r)* (5) and it is plotted in Fig. 4B, 4E and 4H. $P(r)$ is the real-space representation of the particle geometry, with "r" being the chord length between two randomly chosen points. $P(r)=0$ for $r=0$ and for $r>r_{max}$. $P(r)$ data are proportional to the probability of finding two scattering points within VWF that is separated by the distance r. Once *P(r)* is determined, the next step involves conversion of real-space $P(r)$ data into reciprocal space results, i.e. the $I(q)$ versus q plot. This is done by using fourier transform (10, 11):

$$I(q) = 4\pi \int_{o}^{r\,\max} P(r)\frac{\sin(qr)}{qr}\,dr \qquad \text{(A1)}$$

The intensity data are presented in Fig. 4C, 4F and 4I of the main manuscript. In the case where the angle between the rods was varied (case A above), the angle (2φ) in the protomer unit was varied. In this case, $I(q)$ vs. q was independently determined for each of the φ values and the results of selected φ's is shown in Fig. 4C. In the second case where the position of domains within the globular-section of VWF were varied (Fig. 4D), the $I(q)$ vs q plot were determined for a range of φ values from 12º to 84º, and then the average intensity plot was generated by weighting various $I(q)$ for individual φ's using a Gaussian distribution. These φ-averaged $I(q)$ data are presented in Fig. 4F of the main manuscript. Similar calculations were performed for multimeric/tetramer VWF shown in Fig. 4G. Here, the scattering from tetramer VWF at fixed φ was compared to that from dimeric protein at the same φ (Fig. 4 H, 4I)

The computer model described above was validated against various data in published literature. Figures describing these validation steps are not being provided here since this is not the focus of the current paper. Briefly, we validated our computer program against: i) defined

shapes including spheres, prolate and oblate ellipsoids of different dimensions. The distance distribution function, *P(r)*, for these shapes generated in our program compared favorably with analytical solutions published elsewhere (12). Further, the intensity plots ($I(q)$ vs q) we generated matched results generated using small angle scattering software provided by NIST. ii) We also validated the simulation results against computational results predicted for a symmetric dimeric model protein, fibrinogen (10). In these computer modeling, the distance distribution function $P(r)$ from our program matched the results of the previous publication, and the intensity profile generated in the current program also matched over the entire q-range from 0.01-2/nm. iii) Finally, our computer model of dimeric/protomer VWF reasonably fits experimental data on protomer VWF measured using small angle neutron scattering (2) (Supplemental Figure S2).

SUPPLEMENTAL REFERENCES

1. Glinka, C. J., J. G. Barker, B. Hammouda, S. Krueger, J. J. Moyer, and W. J. Orts. 1998. The 30 m small-angle neutron scattering instruments at the National Institute of Standards and Technology. Journal of Applied Crystallography 31:430-445.
2. Singh, I., H. Shankaran, M. E. Beauharnois, Z. Xiao, P. Alexandridis, and S. Neelamegham. 2006. Solution structure of human von Willebrand factor studied using small angle neutron scattering. J Biol Chem 281:38266-38275.
3. Porcar, L., Hamilton,W.A.,Butler,P.D. 2002. A vapor barrier Couette shear cell for small angle neutron scattering measurements. Review of Scientific Instruments 73:2345-2354.
4. Kline, S. R. 2006. Reduction and analysis of SANS and USANS data using IGOR Pro. Journal of Applied Crystallography 39:895-900.
5. Doherty, G. K., and G. A. Poland. 1998. MC_DDF, a computer program for generating distance distribution functions from model particles using Monte Carlo chord sampling. Journal of Applied Crystallography 31:83-90.
6. Fowler, W. E., L. J. Fretto, K. K. Hamilton, H. P. Erickson, and P. A. McKee. 1986. Substructure of human von Willebrand factor. J Clin Invest 76:1491-1500.
7. Fretto, L. J., W. E. Fowler, D. R. McCaslin, H. P. Erickson, and P. A. McKee. 1986. Substructure of human von Willebrand factor. Proteolysis by V8 and characterization of two functional domains. J Biol Chem 261:15679-15689.
8. Bienkowska, J., M. Cruz, A. Atiemo, R. Handin, and R. Liddington. 1997. The von willebrand factor A3 domain does not contain a metal ion-dependent adhesion site motif. J Biol Chem 272:25162-25167.
9. Emsley, J., M. Cruz, R. Handin, and R. Liddington. 1998. Crystal structure of the von Willebrand Factor A1 domain and implications for the binding of platelet glycoprotein Ib. J Biol Chem 273:10396-10401.
10. Hansen, S. 1990. Calculation of Small-Angle Scattering Profiles Using Monte-Carlo Simulation. Journal of Applied Crystallography 23:344-346.
11. Hansen, S. 2003. Estimation of chord length distributions from small-angle scattering using indirect Fourier transformation. Journal of Applied Crystallography 36:1190-1196.
12. Glatter, O. 1979. Interpretation of Real-Space Information from Small-Angle Scattering Experiments. Journal of Applied Crystallography 12:166-175.

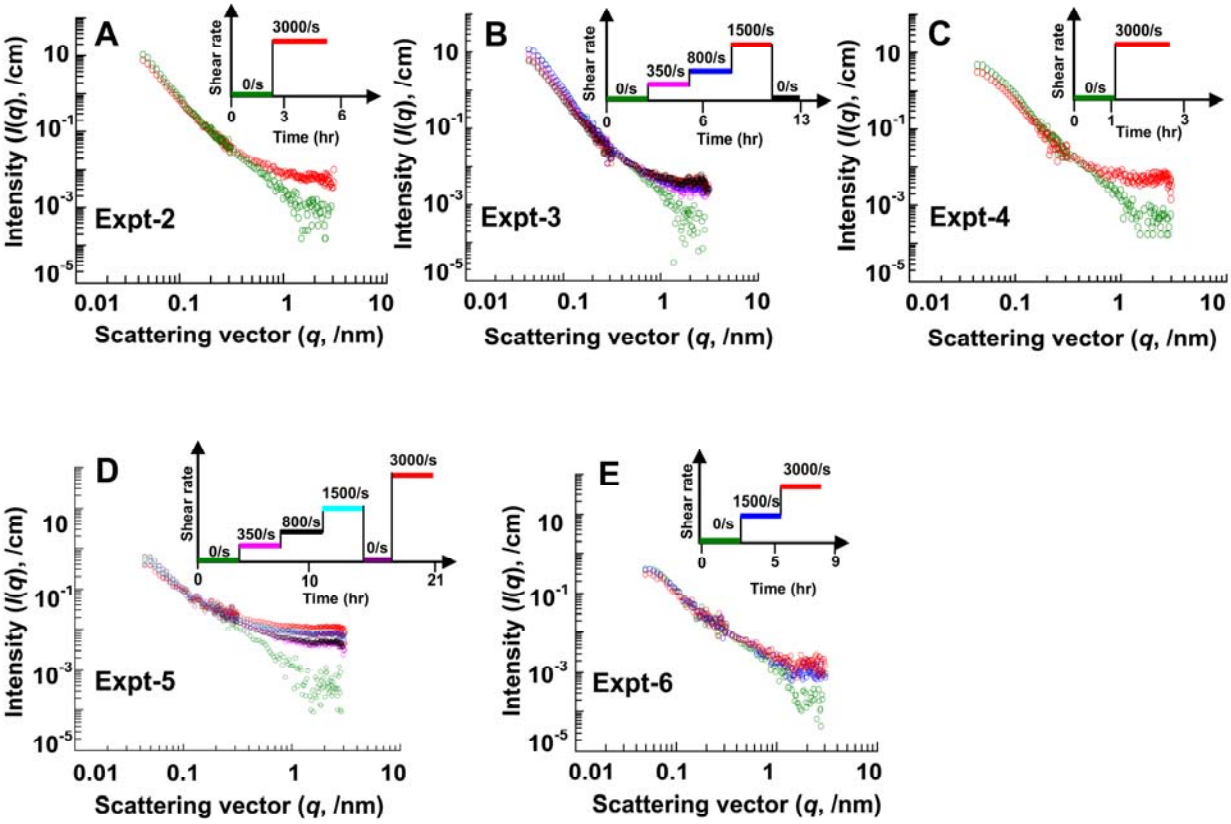

SUPPLEMENTAL FIGURE S1

Shear studies with human VWF. Five independent runs (shown in panels A-E) were performed with VWF isolated from human plasma cryoprecipitate. The experimental protocol is identical to that in Figure 2 of the main manuscript. Inset in each panel presents details on the shear-profile applied and the duration of the experiment. In each run, a decrease in intensity at low-q (q<0.08/nm) and an increase in scattering intensity at high-q (q>0.6/nm) was observed. Changes in scattering at high-q were lower in panel E compared to other runs. Stopping shear (panels B, D) did not result in the return of scattering intensity to levels prior to shear application, and this suggests that structural changes observed were not reversible. Changes in scattering were observed at shear rates down to 350/s (panels B, D). 0.6% agarose gel electrophoresis of VWF followed by western blotting was performed either just prior to or immediately following each of these experimental runs and these studies did not reveal any obvious differences in the multimer distribution of the protein among the runs.

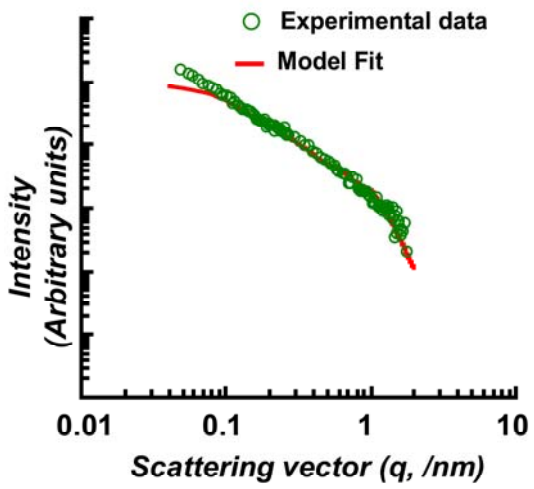

SUPPLEMENTAL FIGURE S2

Comparison of experimental scattering profile (dimeric VWF) with the computer model (also dimeric VWF) show semi-quantitative agreement.